I. R. Ashman[1] and D. R. Faulkner[1]

[1]Department of Earth, Ocean, and Ecological Sciences, University of Liverpool, Liverpool, UK

Corresponding author: Isabel Ashman (isabel.ashman@liverpool.ac.uk)

Key Points:

- Dilatancy with increasing slip velocity is seen for fault gouges ranging from 100 wt% quartz to 100 wt% clay.
- Dilatancy is at a maximum in the quartz-rich, clay-poor gouges, rather than in the end member compositions.
- Increasing clay content systematically decreases the gouge frictional strength and promotes velocity strengthening behaviour.

Abstract (250 words)

Mature fault cores are comprised of extremely fine, low permeability, clay-bearing gouges. Saturated granular fault materials are known to dilate in response to increases in sliding velocity, resulting in significant pore pressure drops that can suppress instability. Up to now, dilatancy has been measured only in clay-poor gouges. Clay minerals have low frictional strengths and, in previous experiments, even small proportions of clay minerals were shown to affect the frictional properties of a fault. It is important, therefore, to document in detail the impact of the proportion of clay on the frictional behaviour and dilatancy of fault rocks. In this work, a suite of triaxial deformation experiments elucidated the frictional behaviour of saturated, synthetic quartz-clay (kaolinite) fault gouges at effective normal stresses of 60 MPa, 25 MPa and 10 MPa. Upon a 10-fold velocity increase, gouges of all clay-quartz contents displayed measurable dilatancy with clay-poor samples yielding comparable changes to previous studies. Peak dilation did not occur in the pure quartz gouges, but rather in gouges containing 10 to 20 wt% clay. The clay content of the simulated gouges was found to control the gouge frictional strength and the stability of slip. A transition occurred at ~40 wt% clay from strong, unstably sliding quartz-dominated gouges to weak but stably sliding clay-dominated gouges. These results indicate that in a low permeability, clay-rich fault zone, the increases in pore volume could generate pore-fluid pressure transients, contributing to the arrest of earthquake nucleation or potentially the promotion of sustained slow slip.

Plain Language Summary

The strength of faults is dependent on the fluid pressure contained within the pore space of fine-grained fault rocks on which fault slip events such as earthquakes occur. When slip velocity increases at the start of an earthquake, the fault rocks dilate, thereby reducing the fluid pressure and consequently strengthening the fault. If this strengthening is sufficient, an earthquake may arrest. Clay minerals are commonly present within faults, but previous measurements of fault volume changes have focused on clay-poor materials. In this study,

a series of experiments simulated the conditions within a tectonic fault in the Earth's crust. The experiments focused on the effect of changing the proportion of clay on the strength, slip behaviour and volume changes of the fault material. All of the experiment materials experienced measurable volume changes that would change the pressure, and therefore the strength, of the fault. Fault composition was found to control both the strength and slip behaviour of the fault. Clay-poor materials were stronger and more likely to initiate earthquake slip, whereas the clay-rich materials were weaker and slip via steady creep. This study provides essential insight and data towards understanding the slip behaviour of faults, from slow fault creep to earthquakes.

1 Introduction

Field observations have shown that mature fault zone cores contain a significant proportion of clay minerals, such as the MTL in Japan (Jefferies et al., 2006; Wibberley and Shimamoto, 2003), the San Andreas Fault including the Punchbowl Fault in USA (French and Chester, 2018; Logan and Chester, 1987), and the Alpine Fault Zone in New Zealand (Toy et al., 2015). The presence of clay minerals has the potential to influence the seismic cycle, and earthquake nucleation in particular, through the frictional strength and stability of the gouge, and pore fluid pressure changes resulting from dilation or compaction during slip velocity transients (Byerlee 1978; Segall and Rice 1995; Faulkner et al. 2018). While the effect of clay content on the bulk frictional strength and permeability of fault gouges is relatively well documented (Brown et al., 2003; Crawford et al., 2008; Giorgetti et al., 2015; Ikari et al., 2007; Logan and Rauenzahn, 1987; Lupini et al., 1981; Moore and Lockner, 2011; Ruggieri et al., 2021; Takahashi et al., 2007; Tembe et al., 2010; Zhang et al., 2020), the effect of dilatancy induced by increasing slip velocity on frictional stability, particularly in clay-rich gouges, is poorly documented.

The role of pore fluid pressure in determining fault shear resistance ( ) is described using the effective pressure law:

$$\tau = \mu\,(\sigma_n - p) \quad (1)$$

where is the coefficient of friction, $_n$ is normal stress and p is pore pressure (von Terzhagi, 1936). Thus, by increasing the pore pressure, the apparent strength of a brittle fault decreases (Ougier-Simonin and Zhu, 2013), or vice-versa. Given the low compressibility of aqueous fluid, even small changes in the pore volume of a shearing fault gouge during changes in slip velocity will produce large fluid pressure variations. (Morrow and Byerlee, 1989; Rudnicki and Chen, 1988). The dilation and compaction of granular materials is accredited to changes in the packing arrangement of the grains (Mead, 1925; Reynolds, 1885). Slip velocity increases are accompanied by dilation of the sample material and a pore pressure drop, whereas slip velocity decreases show compaction of material and pore pressure increases (Brantut, 2020; Lockner and Byerlee, 1994; Morrow and Byerlee, 1989; Proctor et al., 2020; Rathbun and Marone, 2013; Samuelson et al., 2009). The timescale of pore pressure changes due to dilatancy or com-

paction depends on the competition between the changes in pore pressure and the drainage of pore fluid away from sites of excess pressure (Faulkner et al., 2018).

Previous friction experiments focused on dilatancy have typically used quartz-rich sands and powders (Lockner and Byerlee, 1994; Rathbun and Marone, 2013; Samuelson et al., 2009) or studied the initiation of a shear fracture in intact material and subsequent slip (Brantut, 2020; Proctor et al., 2020). In contrast, mature fault cores consist of extremely fine-grained fault gouges that are typically rich in clay minerals and have very low permeabilities, from 10^{-18} m^2 to 10^{-22} m^2 (Chester et al., 1993; Crawford et al., 2008; Faulkner et al., 2003; Faulkner and Rutter, 2000; Ikari et al., 2009; Morrow et al., 1984). Low permeabilities in clay-rich fault materials increases the timescales of the pore pressure changes and their significance in terms of fault shear strength and behaviour.

Dilation of fault material could arrest a nucleating rupture due to a drop in pore pressure, which would increase the apparent shear strength of the fault. Dilatancy in response to slip velocity changes could also suppress fully dynamic behaviour leading to the propagation of slow slip earthquakes (SSEs), which can last periods of days to weeks (Frank et al., 2015; Liu, 2013; Rubin, 2008; Segall et al., 2010). SSEs are inferred to occur in regions of elevated pore pressures at close to lithostatic conditions, including plate boundary settings such as the subduction interface or transform faults (e.g. Audet et al., 2009; Frank et al., 2015; Kodaira et al., 2004; Peng and Gomberg, 2010; Saffer and Wallace, 2015). Hence, fault networks that host SSEs could be highly sensitive to pressure fluctuations and stable fault slip may be promoted on otherwise unstable faults (Obara and Kato, 2016; Ougier-Simonin and Zhu, 2013; Peng and Gomberg, 2010). SSE-hosting fault rocks are often rich in clay minerals (e.g. Audet et al., 2009; Frank et al., 2015; Ikari et al., 2015), thus measuring dilatancy in clay-rich gouges is vital to understand whether pore pressure fluctuations will impact fault seismicity.

While the focus in this work is on dilatancy, intrinsic changes in the frictional strength with changes in slip velocity, such as in earthquake nucleation or propagation, are also investigated. Rate and state friction describes the response to slip velocity variations and is quantified by the constitutive law:

$$\mu = \mu_0 + a \ln\left(\frac{V}{V_0}\right) + b \ln\left(\frac{V_0 \theta}{D_c}\right) \quad (2)$$

Where $_0$ is the initial steady state friction coefficient at slip velocity V_0 (ms^{-1}), the velocity after the step change is V (ms^{-1}), a is the direct effect, b is the evolution effect, D_C is the slip weakening distance and is the state variable with units of time (Dieterich, 1979). If the friction stability parameter (a-b) is greater than zero in response to a velocity step increase, the material is designated as velocity strengthening. Velocity strengthening materials cannot nucleate seismic slip because with accelerating slip the material strengthens and so prevents instability. Conversely, a friction stability parameter of less than zero indicates that the material is velocity weakening. Velocity weakening is a prerequisite

for unstable slip due to the material's overall weakening response to slip acceleration. Previous measurements of the stability of clay minerals (Giorgetti et al., 2015; Ikari et al., 2009; Logan and Rauenzahn, 1987; Ruggieri et al., 2021; Saffer and Marone, 2003; Tembe et al., 2010; Zhang et al., 2020) have shown them to be velocity strengthening, although there is a paucity of systematic measurements of how clay content affects stability compared to measurements of the bulk strength. The compilation by Ikari et al. (2011) indicates that there is broad correlation between clay content and higher *(a-b)* values. It is important to document the effect of gouge composition on the friction parameter *(a-b)* alongside the dilatancy in order to understand the relative contributions of intrinsic material effects and pore fluid pressure changes on shear resistance.

In this work, the materials and methods used to perform the experiments are first described. A series of synthetic quartz-kaolinite gouges were produced that cover clay (kaolinite) contents from 0 wt% to 100 wt% and the synthetic gouges were sheared in a conventional triaxial deformation apparatus. The experimental results first describe the pore volume changes that occur in the synthetic fault gouges as a function of the controlled clay content, both during a bulk compaction phase and also in response to steps in the sliding velocity. The changes in the bulk strength and variation of the friction parameter *(a-b)* as a function of clay content are then reported. In the discussion, all the results are compared to existing data from the literature and the controls on dilatancy, gouge strength and stability are considered. Finally, the implications of the dilatancy for natural fault slip for the range of fault materials tested are discussed.

2 Materials and Methods

The materials used for the quartz-kaolinite synthetic fault gouges were Min-U-Sil 15 silica powder from the US Silica Company and KGa-1B kaolinite source clay from the Clay Minerals Society. Kaolinite was the chosen clay mineral for this study as it provides a useful proxy frictionally for non-swelling clays and kaolinite is of common occurrence in fault rocks. Min-U-Sil 15 was chosen for its high purity at >99% silica and the fine grain size sieved to <15 µm. KGa-1B also has a purity of >99% (Vogt et al., 2002) and extremely fine grain sizes with 57 wt% at <2 µm (Pruett and Webb, 1993; Vogt et al., 2002). As quartz and kaolinite have very similar densities (2.65 g/cm^3), the synthetic fault gouges were mixed by weight, which was also representative of the relative volumes. Kaolinite composition was varied by 10 wt% increments to produce 11 samples from 0 wt% to 100 wt% kaolinite. With the aim of producing a well-mixed starting material, 20g of the samples were tumbled as dry powders for a 3-hour period at 68 rpm in a 575 cm^3 volume container. Dry tumbling was chosen because the similar grain sizes and densities of the kaolinite and quartz powders promotes mixing over segregation (Williams, 1968). Microstructural observations of pre-shear gouge samples show a good degree of mixing, with only minor clumping of clay due to a build-up of static charge in intermediate mixtures.

All deformation experiments were conducted using a direct shear configuration in a triaxial deformation apparatus (Figure 1). Using servo-controlled pumps, the apparatus can apply and maintain confining pressures up to 250 MPa and pore fluid pressures up to 200 MPa to an accuracy of 0.007 MPa. The confining and pore fluids used in the experiments were silicon oil and deionised water, respectively. An internal force gauge measures the axial force at a resolution better than 0.05 kN (Mitchell and Faulkner, 2008).

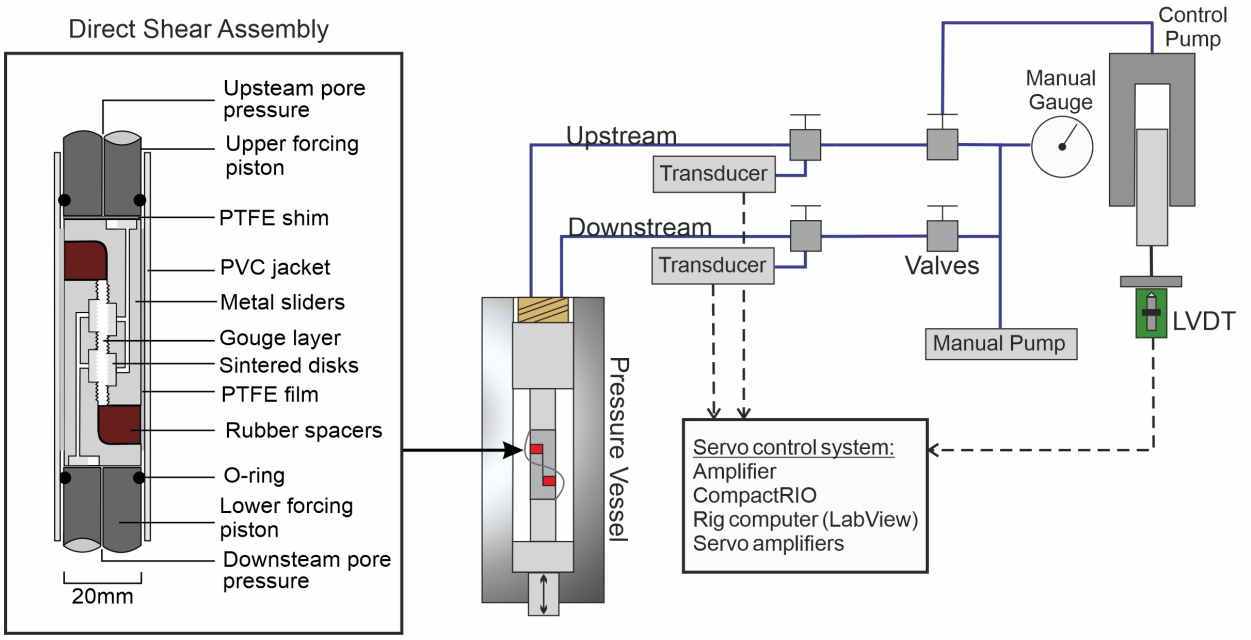

Figure 1: Schematic diagram of the servo-controlled pore pressure control system on the triaxial deformation apparatus (adapted from Mitchell & Faulkner, 2008).

In the experiments, samples of fault gouge were deformed in direct shear sliders (Faulkner et al., 2018; Sánchez-Roa et al., 2016) shown in Figure 1. The dimensions of the direct shear sliders created a sample area of 720 mm^2 and two rubber spacers allowed a maximum load point displacement of 6 mm. Air dry synthetic gouge samples of 1.6 g were pre-compacted by loading at 50 kN perpendicular to the layer using a uniaxial press. This produced samples with initial thicknesses of ~1.3 mm before pressurisation, improved sample cohesion for assembly, and reduced the initial porosity of the gouge. Porous stainless steel disks with permeabilities of 10^{-13} m^2 in the direct shear sliders allowed transfer of pore fluid between the sample and the servo-controlled pore pressure pump (Figure 1).

The synthetic gouge samples were sheared in velocity-step tests at pore pressures held at 40 MPa and effective normal stresses ($_n{}^{eff}$) of 60 MPa, 25 MPa and 10

MPa to represent increasingly overpressured conditions. Samples were initially run at an axial loading rate of 0.3 µm/s for a displacement of 2 mm to bring the sample past yield, where the shear strength of the sample reached steady state. Following the initial yield phase, the sliding velocity was stepped between 0.3 µm/s and 3.0 µm/s every 0.5 mm of load point displacement to a maximum of 5.5 mm. The displacement on the friction curves has not been corrected for machine compliance, which was 75 kN/mm. Permeabilities of the gouge samples were measured at the end of shearing using the pore pressure oscillation technique (Bernabé et al., 2006; Faulkner and Rutter, 2000; Kranz et al., 1990), which returned final permeabilities of 10^{-17} m^2 for quartz-rich gouges to 10^{-20} m^2 for kaolinite-rich gouges. The permeability was not monitored throughout the test as this reduced the capacity to monitor very small changes in pore volume during velocity steps, the technique for which is described next.

Pore volume changes during a test were monitored using the pore pressure control system, shown in Figure 1. The servo-controlled 5000 mm^3 pump adjusted the volume of fluid in the system to maintain the pressure at 40 MPa from measurements in the sample; a pore pressure increase required pore fluid to be extracted into the pump, whereas a pressure decrease required pore fluid to be added to the sample. By monitoring the displacement of the piston in the pore fluid control pump using a high-resolution linear variable differential transformer (LVDT), the equivalent changes in pore volume in the sample were measured (Figure 2). The maximum volume change that the LVDT could measure with one stroke was 200 mm^3 and the measurements were resolvable to 0.01 mm^3. This pore volume monitoring technique (volumometery) included a time-dependent component because the control pump could only respond to pore pressure changes that had diffused out of the gouge sample. In order to assess the potential effect of these transients, the characteristic time (t) for equilibration of pore pressure across the sample was calculated using the thickness of the sample (l) and the hydraulic diffusivity ( ):

$t = \frac{l^2}{\kappa}$ (3)

This returned characteristic times across the range of gouge compositions of 10^{-3} to 1 sec. The synthetic gouges therefore had sufficiently high permeabilities for any pore pressure transients to equilibrate rapidly with the control pump, and thus gave reliable measurements of pore volume changes produced during the velocity steps (180 secs to 1800 secs).

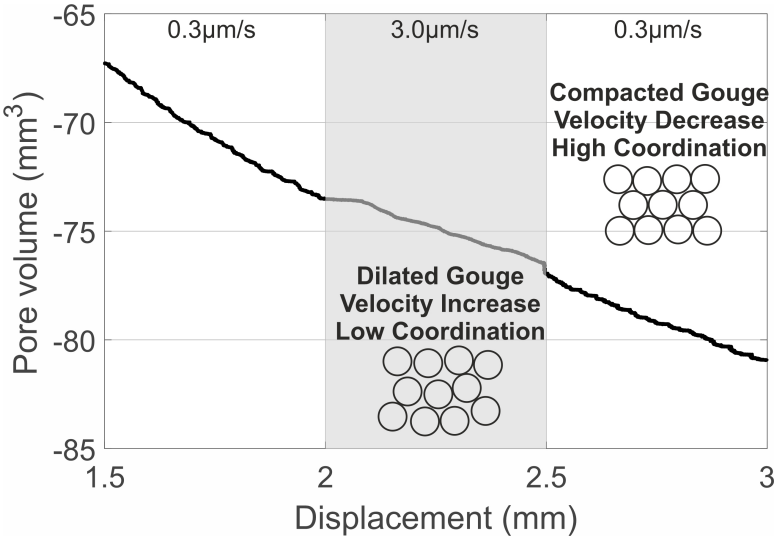

Figure 2: Measured pore volume changes in response to velocity step changes due to changes in packing of a granular material.

To determine the volume changes in response to velocity steps in a reproducible way, the volume curve for an individual velocity step was incrementally adjusted to produce a least-squares fit to the overall compaction trend (see Figure 2 and Appendix for more details). In addition to reporting the measured volume changes, a dimensionless dilatancy parameter is reported for comparison between literature dilatancy data (Samuelson et al., 2009; Segall et al., 2010). normalises the measured volume change (Δvol) to both the total sample volume (vol) and the step change from initial slip velocity (V_0) to the increased slip velocity (V):

$$\varepsilon = \frac{\left(\frac{vol}{\mathrm{vol}}\right)}{\log \frac{V}{V_0}} \quad (4)$$

This removes the effects of sample volume and the scale of velocity step change from and allows direct comparison between published datasets.

Rate and state frictional parameters of the gouges were determined using the program RSFit3000 (Skarbek and Savage, 2019) that uses a non-linear least squares routine (Reinen and Weeks, 1993) to fit the experimental data to obtain the direct effect a, evolution effect b, and the slip weakening distance D_c from imposed velocity step changes. The stiffness (k) of the apparatus is also a fitting parameter (Noda and Shimamoto, 2009). In RSFit3000, the state evolution was described using the aging law (Ruina, 1983):

$$\frac{\mathrm{d}}{\mathrm{dt}} = 1 - \frac{\mathrm{V}}{D_c} \quad (5)$$

This experimental framework that measures the gouge frictional strength, stability and dilatancy has been developed so that it can be applied to a wider

range of fault gouge compositions.

3 Results

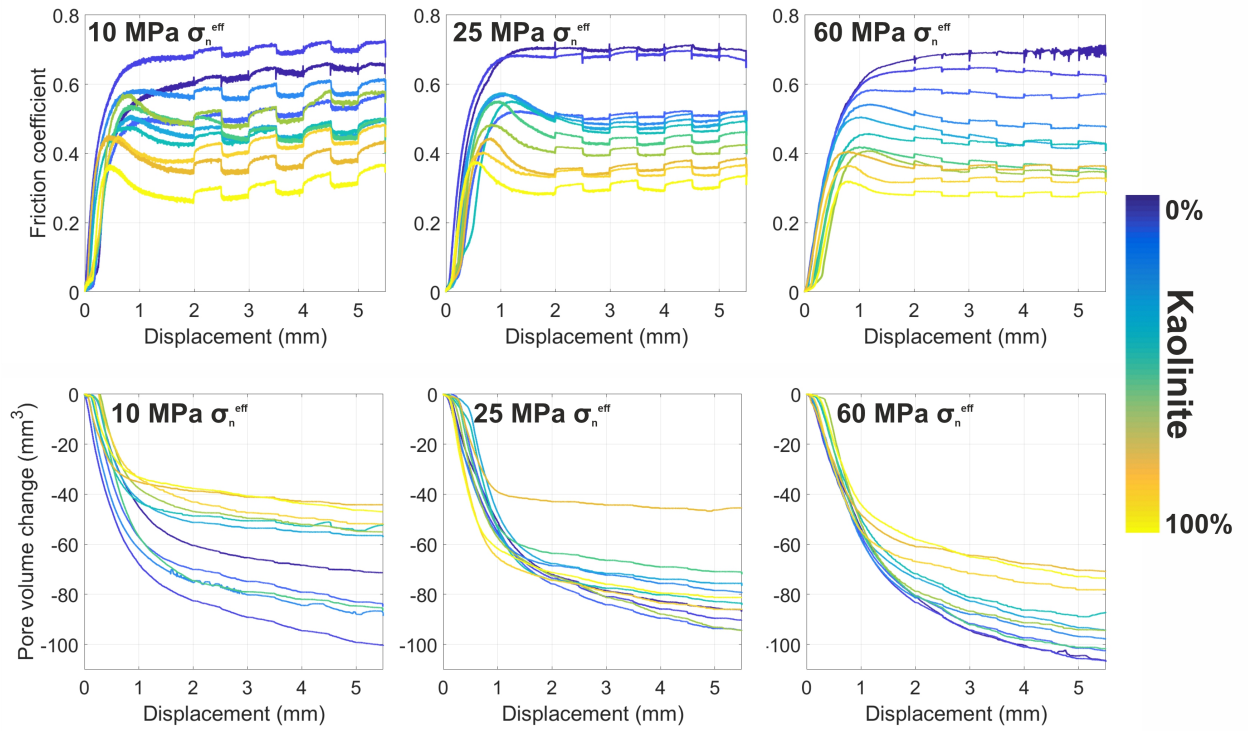

Figure 3: Summary of friction results (top) and volume change results (bottom) for velocity step test experiments at 10MPa, 25MPa and 60MPa effective normal stresses with incremental changes in gouge kaolinite content.

Prior to the onset of sliding, the samples were pressurized, which resulted in them compacting hydrostatically (Figure 3). Upon commencement of sliding, a phase of shear enhanced compaction occurred. The majority of shear enhanced compaction occurred prior to the yield phase of the tests. The kaolinite-rich gouges saw less compaction prior to the yield phase than the kaolinite-poor gouges, wich is in line with previous studies that showed that more hydrostatic compaction occurred in the clay-rich gouges (e.g. Crawford et al. 2008). All gouges continued to compact after yield, although at a slower rate. The total amount of compaction, shown in Figure 4, was sensitive to the kaolinite content of the gouge and the test $_n^{\text{eff}}$. Increasing the kaolinite content led to a decrease in overall compaction, such as at 60 MPa $_n^{\text{eff}}$ the 0 wt% kaolinite gouge experienced 106 mm^3 of compaction compared to 79 mm^3 of compaction for the 100 wt% kaolinite gouge. Increasing $_n^{\text{eff}}$ increased the overall shear enhanced compaction of a sample. The 0 wt% kaolinite gouge underwent 71 mm^3, 86 mm^3 and 106 mm^3 pore volume reduction across the increasing effective normal stresses

(Figure 4).

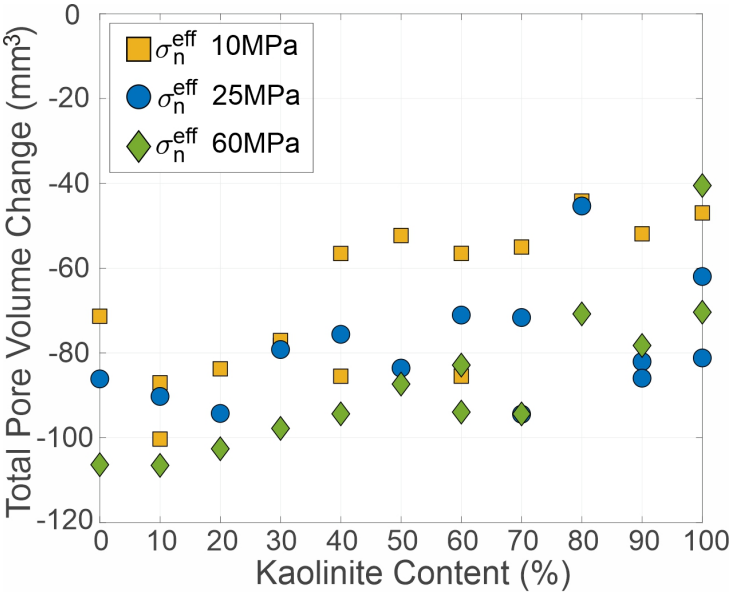

Figure 4: Experimental shear-enhanced compaction of synthetic fault gouges at 5.5mm displacement.

Dilation and compaction in response to velocity step changes that deviated from the overall compaction trend were observed in all the quartz-kaolinite gouges (Figure 5). Dilation always followed an increase in slip velocity and compaction always followed a decrease in slip velocity. The compaction following a velocity decrease was greatest in the 0 wt% kaolinite (100 wt% quartz) gouge but was then consistent across the gouge compositions containing more than 10wt% kaolinite. The dilation was greatest at kaolinite contents of 10-40 wt% with a decreasing trend towards the two end-member gouge compositions. Unlike the shear enhanced compaction results, there was no systematic effect from varying the $_n^{\text{eff}}$ on the dilatancy behaviour. The dilatancy was asymmetric as pore volume increases after velocity upsteps were always greater than pore volume decreases following velocity downsteps. For example at 25 MPa $_n^{eff}$ the 10 wt% kaolinite had a mean dilation of 1.0 mm^3 and a mean compaction of 0.2 mm^3.

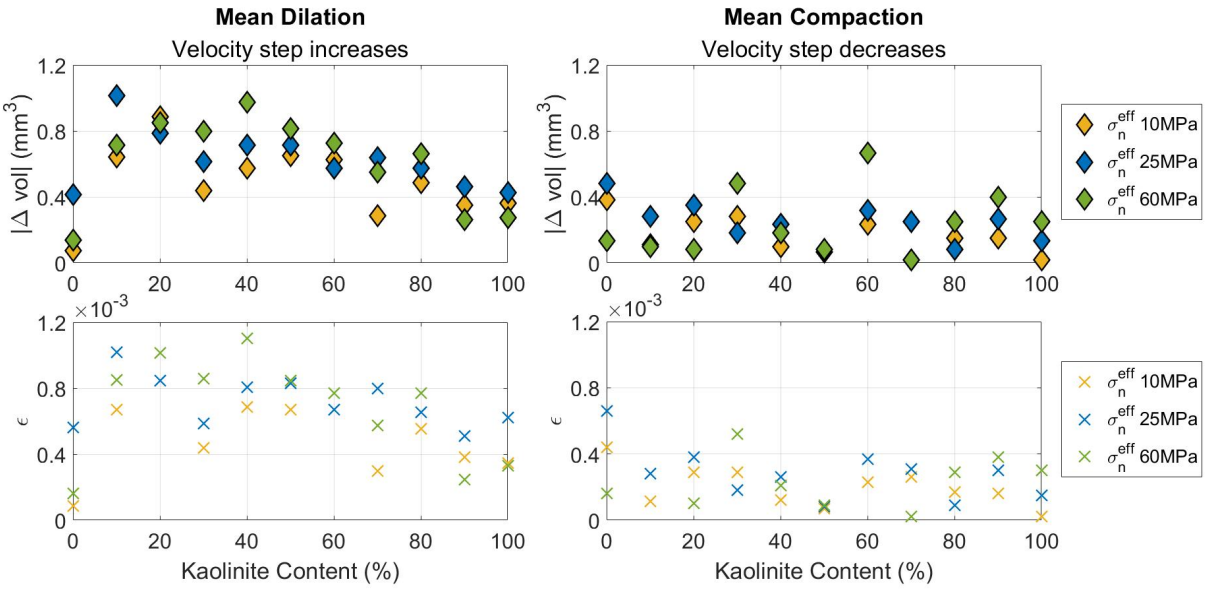

Figure 5: Measured (top) and normalised (bottom) experimental dilation and compaction in response to velocity-step changes in synthetic fault gouges.

All of the synthetic gouges reached a steady state yield strength following the initial 2 mm of load point displacement (*Figure 3*). The frictional strength of the synthetic gouges showed a strong dependence on the kaolinite content (Figure 6). The frictional strength of the gouges at the end of the tests, as shown in Figure 6, decreased with increasing kaolinite content from 0.689 for 0 wt% kaolinite to 0.275 for 100 wt% kaolinite at 60 MPa $_{n}^{\text{eff}}$. This negative trend was non-linear; frictional strength decreased steeply to 40 wt% kaolinite, beyond which the decreasing trend shallows.

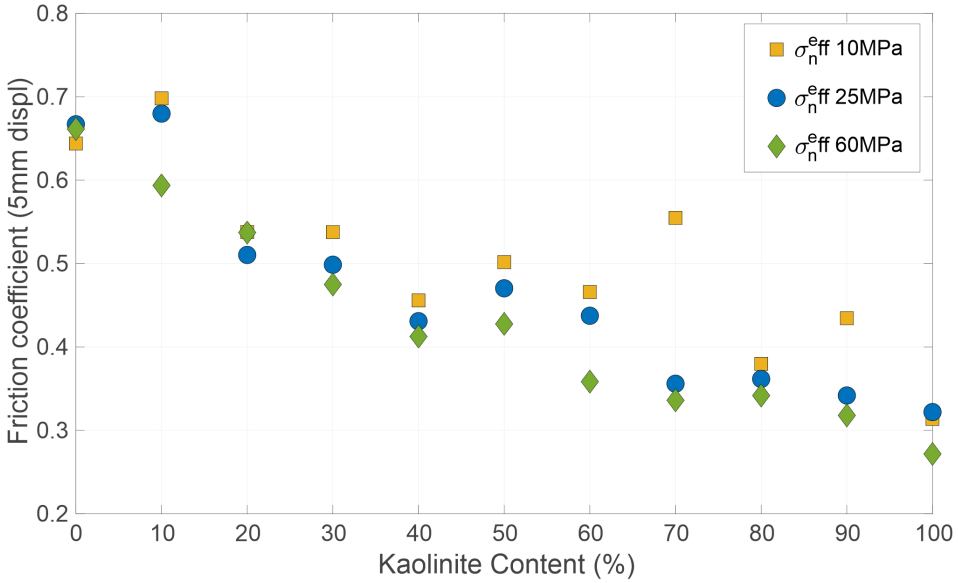

Figure 6: Experimental frictional strength of synthetic fault gouges after 5mm of load point displacement.

The frictional parameter *(a-b)* was also strongly dependent on the kaolinite content (see Figure 7). Only gouges with 0 wt% kaolinite displayed velocity weakening behaviour in response to velocity steps, with the test at the highest effective normal stress (60 MPa) producing stick-slip instabilities at the end of the test (Figure 3). All gouges that contained any amount of kaolinite showed velocity strengthening behaviour. As with the gouge strength, the *(a-b)* results showed a change in sensitivity to gouge clay content. Below 40 wt% kaolinite, *(a-b)* increased with increasing kaolinite content but beyond 40 wt% kaolinite *(a-b)* was less dependent on the kaolinite content. The stability of the synthetic gouges was also strongly affected by the effective normal stress, as shown in Figure 7. Decreasing $_n^{\text{eff}}$ decreased b to negative values, leading to larger *(a-b)* values and greater stability of sliding in the gouges. For example, in the 100 wt% kaolinite gouge *(a-b)* increased from 0.003 at 60 MPa $_n^{eff}$ to 0.012 at 10 MPa $_n^{eff}$.

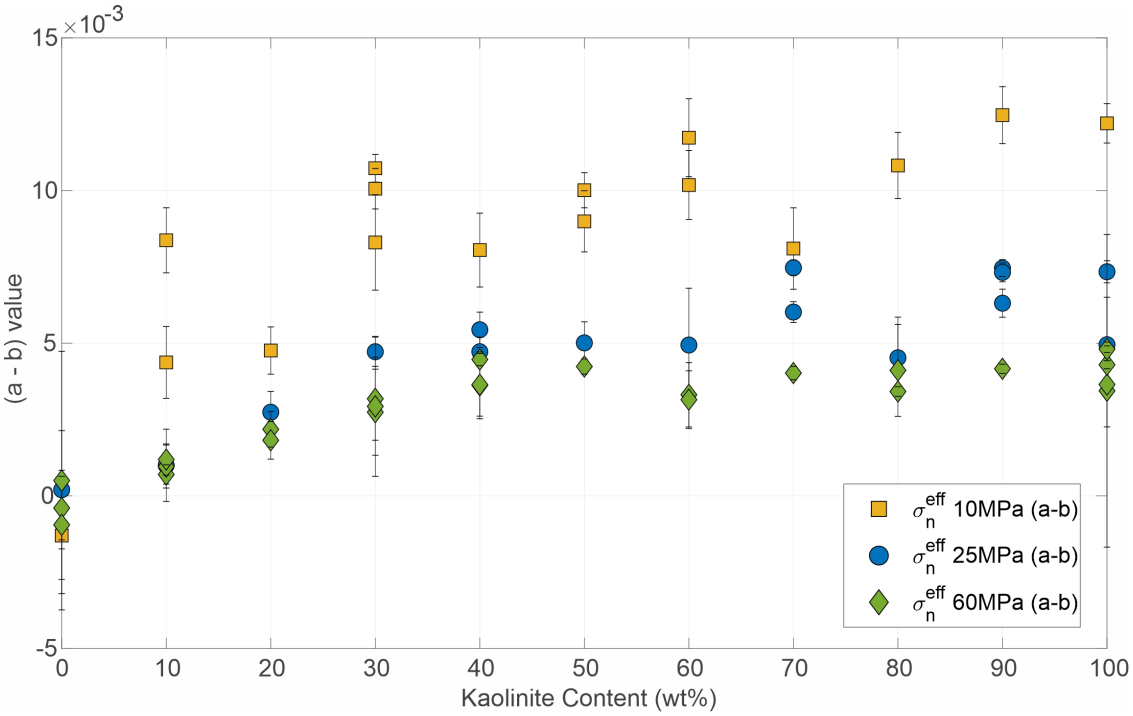

Figure 7: Experimental rate and state stability of synthetic fault gouges from a velocity step increase at 5mm load point displacement. A material is velocity weakening when (a-b)<0 or velocity strengthening when (a-b)>0.

Samples of the synthetic gouges were recovered post-shearing for observations of the microstructures using a scanning electron microscope (Figure 8). The gouge microstructures showed a change with increasing kaolinite content from localised shear zones to more diffuse deformation across the gouge layer. In the clay-poor (0-10 wt% kaolinite) gouge samples, there was evidence of grain comminution and cracking in localised shear zones, as shown by the significant decrease in quartz grain size (Figure 8, a & b). Shear across the layer had been accommodated by a series of R_1 Riedel and shear-direction parallel Y-shears. The Y-shears were located on the periphery of the gouge layer, close to the interface with the direct shear slider surface (sometimes called boundary or B shears). As the kaolinite content increased, the quartz grains became increasingly more isolated and the microstructure changed from a clast-supported to a matrix-supported framework. From intermediate kaolinite contents (>30 wt%), Riedel shears and evidence of grain comminution became increasingly rare. The lack of a throughgoing Y-shear was shown by the 80 wt% kaolinite sample in Figure 8 (g), as the sawtooth interface between the shear slider and the gouge had been preserved.

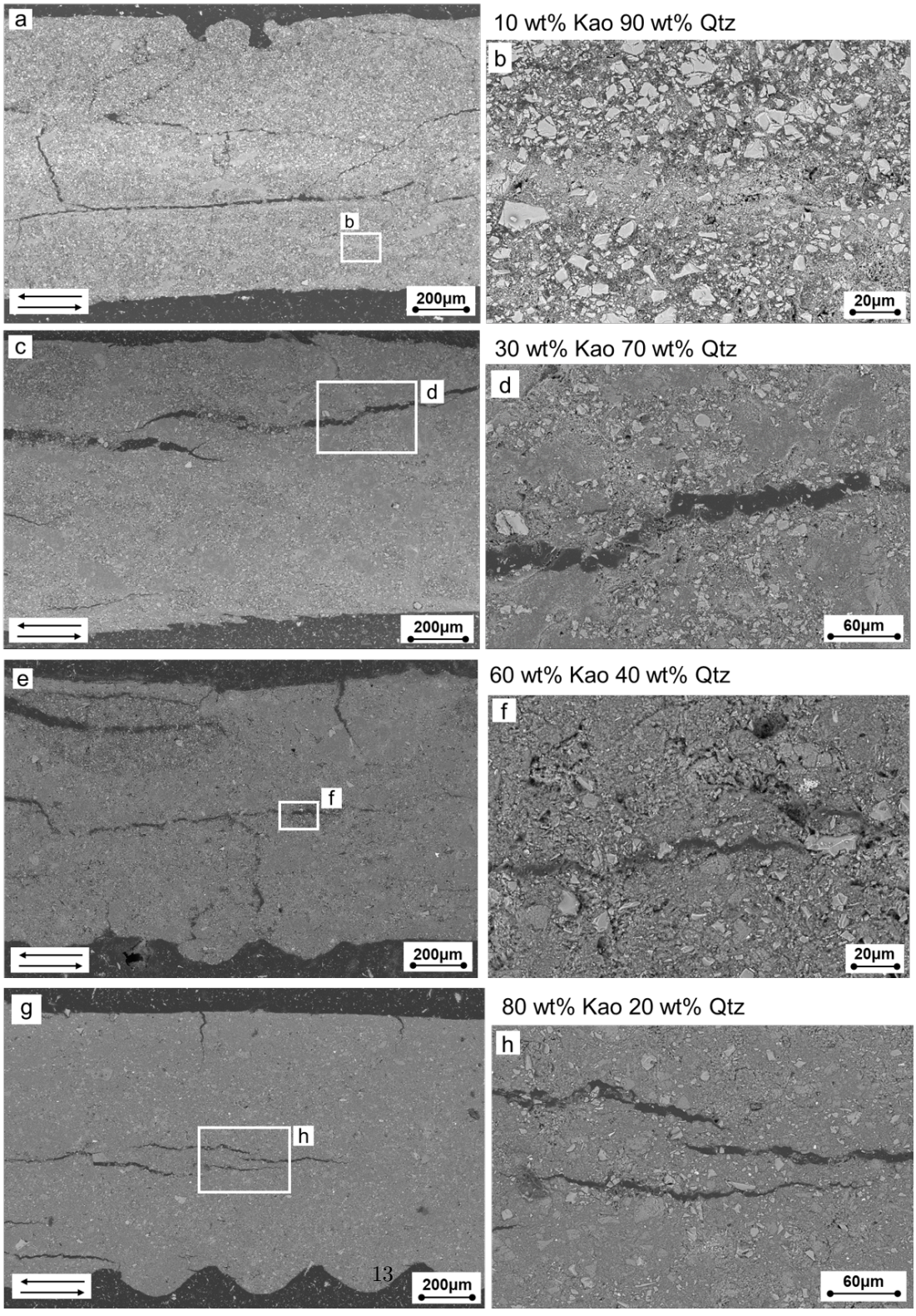
a
b
200µm
10 wt% Kao 90 wt% Qtz
b
20µm
c
d
200µm
30 wt% Kao 70 wt% Qtz
d
60µm
e
f
200µm
60 wt% Kao 40 wt% Qtz
f
20µm
g
h
200µm
80 wt% Kao 20 wt% Qtz
h
60µm

Figure 8: Back scatter SEM images of sheared samples of synthetic kaolinite-quartz gouges. The kaolinite content of the examples increases from 10 wt% (a,b) to 30 wt% (c,d), 60 wt% (e,f) and 80 wt% (g,h).

4 Discussion

Controls on Dilatancy

Previous measurements of dilatancy in granular materials have focused on quartz-rich materials. The dataset presented in this work greatly expands the compositional range of measurements to include clay-rich and clay-only materials (Figure 9). The results show that gouge composition is a factor on the magnitude of dilatancy. Figure 9 also shows that maximum occurs not in the quartz-only gouges, but in the quartz-clay mixtures with 10-20 wt% clay. Changes in composition of a gouge incorporates multiple factors that may affect the scale of dilatancy, such as grain size, grain shape and roughness. However, the dilatancy of the very fine-grained clay material was very similar or exceeded the dilatancy in the coarser-grained quartz. The maximum dilatancy at intermediate clay proportions likely results from changes in the mechanisms that accommodate shear, as compared to the end member gouges. Firstly, the smearing of a weak phase along grain contacts reduces the shear strength of a granular material, even at small proportions (5 wt%) of the weak phase (Rutter et al., 2013). The addition of very fine-grained clay may act to disrupt quartz-quartz contacts through grain sliding on the clays . The mechanisms of grain rolling and dilation would be promoted over cracking of the quartz grains. Secondly, Rathbun and Marone (2010) proposed dilatancy increases with the width of the zone of active shear. The proportion of kaolinite to quartz increases the width of the active shear zone. The Min-U-Sil quartz powder forms highly localised R_1 Riedel shears in triaxial deformation experiments (e.g. Bedford and Faulkner, 2021), however, with increasing kaolinite content, the gouges deforms in broader, less localised shear zones and localized shears become rare (Figure 8). Dilatancy may be greater in the kaolinite-rich gouge mixtures due to the more distributed shear that occurs across the gouge layer in comparison to the quartz-only gouge.

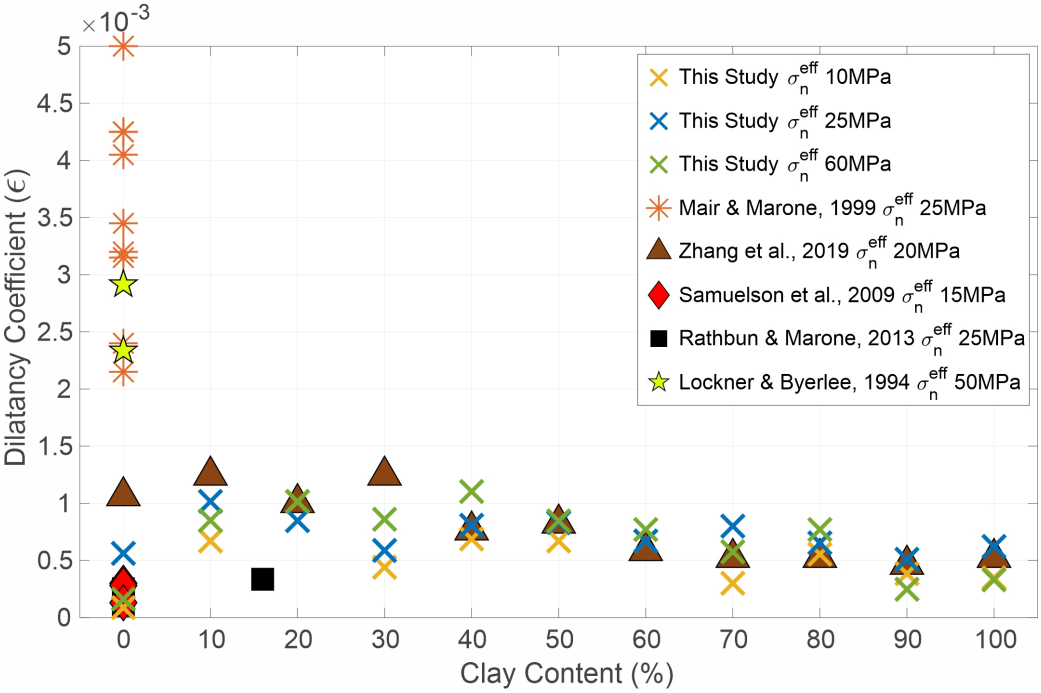

Figure 9: Pore volume increase (dilation) of experimental fault gouges normalised to sample volume and velocity step change ( ).

The dilatancy results also showed a distinct asymmetry between the scale of dilation and compaction for velocity up-steps versus down-steps (Figure 5). The quartz-only gouges showed equivalent or slightly more compaction than dilation in response to velocity step changes, whereas all kaolinite-bearing gouges showed greater dilation than compaction. The asymmetry in the dilatancy results suggests that the strain rate history of the gouge affects the overall pore volume change in a sample. A velocity-stepping experiment produced less overall compaction than a constant velocity experiment, due to this asymmetry. In the measurements by Rathbun & Marone (2013) on quartz powders and clay-bearing glacial tills, both symmetry and asymmetry in the frictional curves and volume changes were observed. The asymmetry in their data is the opposite to that seen in this study, with compaction greater than dilation. Rathbun & Marone (2013) posit that dilation occurs only in the active slip zone and requires both shear strain and interparticle slip, but compaction occurs across the whole layer and only requires a change in stress to occur. The broad and diffuse microstructures in the kaolinite-bearing gouges of this study (Figure 8) may incorporate a higher proportion of the sample that dilates at a slip velocity step increase. The inversion of the asymmetry may result from the higher clay content and different grain size ranges in the gouges of this study, as this subsequently created differences in the gouge microstructures to the experiments done by Rathbun & Marone (2013).

Controls on frictional behaviour

Previous experimental investigations have already established clay content as a primary control on the frictional strength of fault gouges, as summarised in Figure 10 (Brown et al., 2003; Crawford et al., 2008; Ikari et al., 2009; Logan and Rauenzahn, 1987; Moore and Lockner, 2011; Takahashi et al., 2007; Tembe et al., 2010). The data produced in this investigation adds measurements of rate and state friction parameters in greater detail across the compositional range of kaolinite-bearing fault gouges (e.g. Crawford et al., 2008) by controlling kaolinite-quartz content in 10 wt% increments between the two end member compositions. The non-linear decreasing trend of frictional strength with kaolinite content concurs with other deformation experiments using kaolinite (Crawford et al., 2008) and other clays, including: smectites (Ikari et al., 2007; Logan and Rauenzahn, 1987; Takahashi et al., 2007; Tembe et al., 2010; Zhang et al., 2020), illite (Brown et al., 2003), and talc (Moore and Lockner, 2011). Kaolinite-quartz mixtures display a 2-phase decrease in frictional strength with a transition at ~40 wt% (see Figure 10).

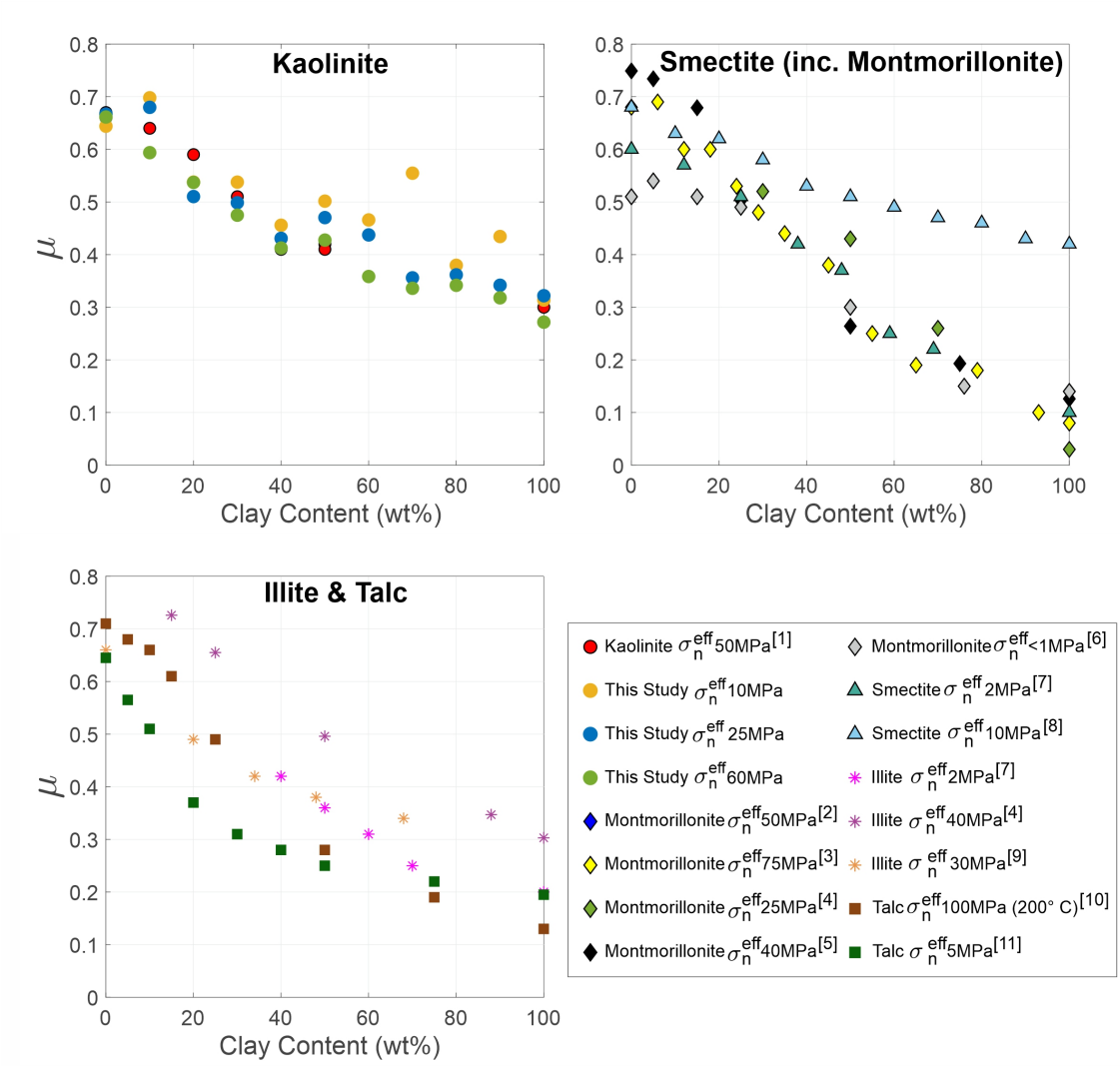

Figure 10: Experimental frictional strengths of quartz-clay gouges. Literature sources: [1] Crawford et al., 2008; [2] Logan & Rauenzahn, 1987; [3] Takahashi et al., 2007; [4] Ikari et al., 2007; [5] Tembe et al., 2010; [6] Lupini et al., 1981; [7] Brown et al., 2003; [8] Zhang et al., 2020; [9] Ruggieri et al., 2021; [10] Moore & Lockner, 2011; [11] Giorgetti et al., 2015.

Grain packing models (e.g. Lupini et al., 1981; Marion et al., 1992; Takahashi et al., 2007) can be used to understand the changes in frictional strength of a gouge due to the gouge's composition. For gouges with low clay contents, an interconnected framework of quartz grains supports the applied stresses and governs the gouge deformation (Ikari et al., 2007; Logan and Rauenzahn, 1987; Takahashi et al., 2007). With increasing clay content, the available pore space

within the quartz grain-supported framework will be filled by the finer-grained clay (see Figure 8). Under zero pressure the porosity of the quartz is ~40 % and the clay ~70 %. Hence at ~40 wt% clay, the clay grains fill the available pore space and the gouge strength cannot be supported by quartz grain contacts alone (Takahashi et al., 2007). At clay contents of >40 wt%, quartz-quartz contacts become rare and the applied stresses are supported by an interconnected clay matrix (see Figure 8). When pressure is applied both end members compact, so that the porosity minimum migrates from 40 wt% clay to lower values (Crawford et al. 2008). A 3 phase decrease in frictional strength observed for smectite mixtures was explained using a transitional regime between the quartz- and clay-dominated regimes, which was not observed here (Lupini et al., 1981; Tembe et al., 2010). However, the porosity measurements by Marion et al. (1992) show that porosity is at a minimum between 20 wt% to 40 wt% clay in a quartz sand-kaolinite mixture at effective stresses of 10 MPa to 50 MPa. This broadly fits with the transition in the frictional data from the grain-supported framework of quartz to the matrix-supported framework of clay at ~40 wt% clay in this study.

Across various literature sources, apparatus and experimental parameters, there is consensus that clay minerals typically *display velocity strengthening behaviour (Figure 11).* The consistency of the (a-b) parameter beyond ~40 wt% kaolinite indicates that the frictional response to a velocity-step change is strongly influenced by the kaolinite (Figure 7) and is supported by the microstructural transition from a localized quartz-dominated fabric to a distributed clay-dominated fabric (Figure 8). Quartz is a typically velocity weakening material but the addition of only 10 wt% kaolinite, a typically velocity strengthening material, is enough to change the gouge to weakly velocity strengthening behaviour. In contrast to the frictional strength results, the (a-b) parameter shows not only a strong positive dependence on kaolinite proportion but also on $_{n}^{eff}$. Bedford and Faulkner (2021) report a similar dependence of (a-b) on $_{n}^{eff}$ in quartz powders as is observed in this study. As $_{n}^{eff}$ increases, the friction parameters become more velocity weakening and stick slip behaviour becomes prevalent, although this is not consistent across all reported data.

In this study, the direct effect *(a)* remained constant at ~0.005 at clay proportions >40 wt% across all $_{n}^{eff}$. The increased *(a-b)* parameter at lower $_{n}^{eff}$ was due to changes in the evolution effect *(b)*, which decreased to strongly negative values, with a minimum of -0.0114. Negative b values do not conform to the interpretation of the evolution effect deriving from changes in the contact area (Dieterich, 1979; Li et al., 2011). If the evolution effect is a result of changes in the contact area, contact saturation would occur at $b = 0$ so that a negative b value would imply that the contact area of the grains exceeds saturation (Ikari et al., 2009). Negative b values therefore lend weight to the argument that the frictional aging of grain contacts, through processes such as chemical bonding, controls the friction evolution effect in clay-rich gouges (Li et al., 2011). Mineral surfaces of phyllosilicates commonly have a high surface charge, and so can produce grain contacts with variations in strength dependent on the presence

or absence of absorbed water.

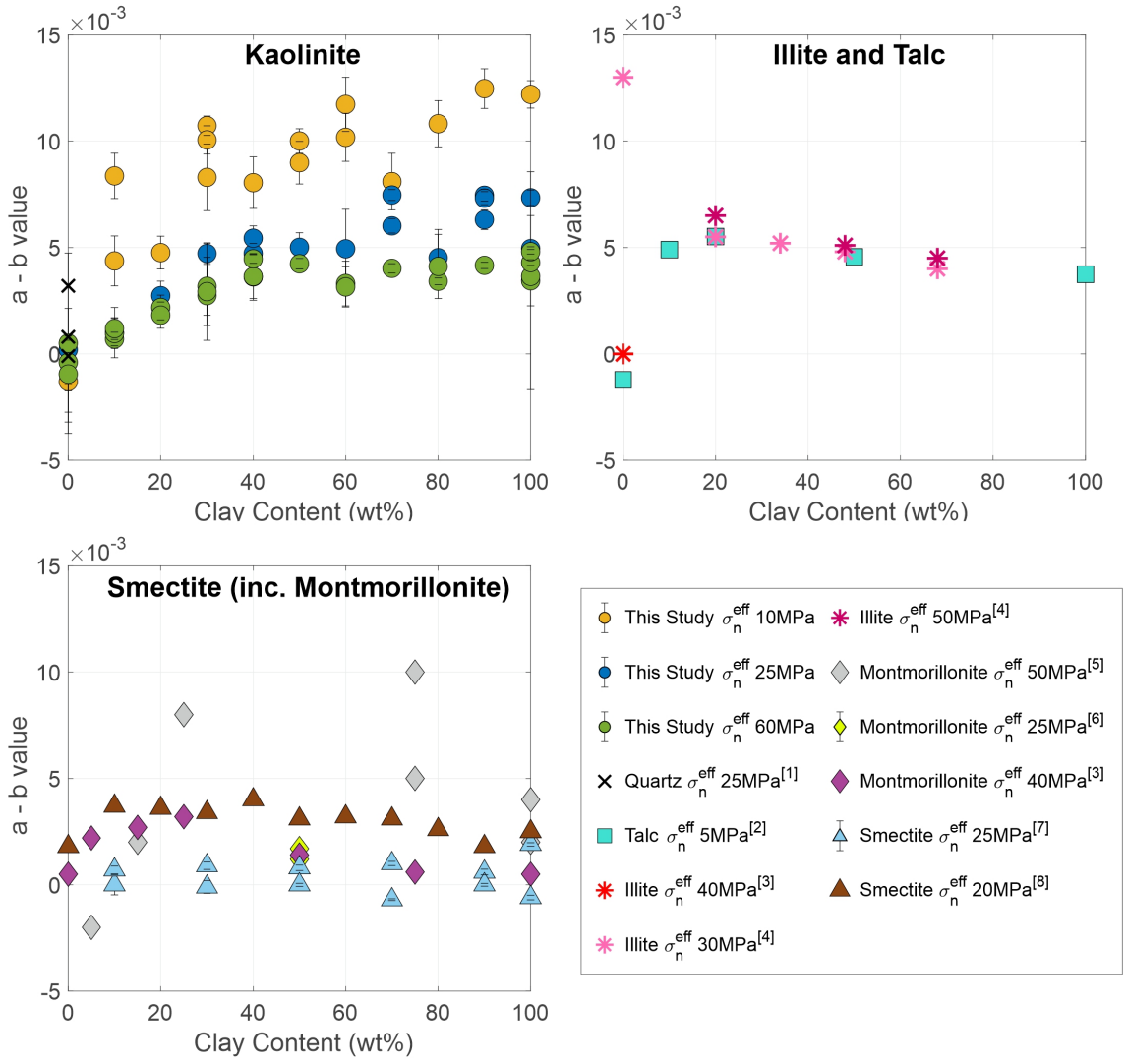

Figure 11: Experimental frictional stability parameters (a-b) from velocity step tests reported from literature sources: [1] Mair & Marone, 1999; [2] Giorgetti et al., 2017; [3] Tembe et al., 2010; [4] Ruggieri et al., 2021; [5] Logan & Rauenzahn, 1987; [6] Ikari et al., 2009; [7] Saffer & Marone, 2003;[8] Zhang et al., 2020.

Implications of gouge dilatancy

Several studies have incorporated dilatancy into models for earthquake nucleation and propagation (e.g. Dal Zilio et al., 2020; Liu, 2013) and rate and state

friction frameworks (Ferdowsi and Rubin, 2020; Heimisson et al., 2021; Rathbun and Marone, 2013; Segall and Rice, 1995). In the results presented here, only the quartz gouges showed velocity-weakening behaviour and could therefore nucleate earthquakes. Consequently, for earthquake nucleation, the pore pressure changes in clay-poor (quartz-rich) gouges are more significant. The dilation in response to acceleration of slip would cause a pore pressure drop and any potential instability would be dampened. Dilatancy in clay-rich gouges would lead to more prolonged pore pressure changes than in clay-poor gouges, because low permeabilities in clay-rich gouges tend towards undrained conditions. However, the weak, velocity strengthening clay-rich gouges will not nucleate instabilities. Instead, dilatancy increases the capacity of more clay-rich regions of faults to arrest growing slip patches during nucleation and earthquake propagation. Current models of fault seismicity have incorporated dilatancy parameters on the order of 10^{-4} to investigate the role of dilatancy in the seismic cycle (Dal Zilio et al., 2020; Heimisson et al., 2021; Liu, 2013; Segall et al., 2010). This study has measured dilatancy in the range of $2\text{x}10^{-4}$ to $1.1\text{x}10^{-3}$ across the full compositional range of quartz to clay content.

In previous investigations (Rathbun and Marone, 2013; Segall and Rice, 1995), attempts have been made to describe the stability of fault slip using both the rate and state friction parameters and the dilatancy parameter. An example from Segall & Rice (1995) defines the stability parameter (E):

$E = \frac{}{\mathrm{b}(\sigma - p)}$ (6)

Where is the compressibility of the material. If $E < 1 - a/b$ it indicates that, under the set conditions, the fault has the potential to host an earthquake, whereas a value of $E > 1 - a/b$ indicates that quasi-static slip behaviour would occur (Segall and Rice, 1995). An alternative method to calculate the effect of dilatancy on fault slip behaviour is to relate the change of steady state shear stress ($_{ss}$) with the natural log of slip velocity (v) to the steady state frictional strength of the material ($_{ss}$) (Segall and Rice, 1995):

$\frac{\partial \tau_{\mathrm{ss}}}{\partial \ln v} = \frac{\mu_{\mathrm{ss}} \varepsilon}{(\sigma - p)\beta}$ (7)

In order to produce instability, this parameter would need to be negative and bring the curve below a critical stiffness criterion (k_{crit}) that is defined for an undrained system as:

$k_{\mathrm{crit}} = \frac{(\sigma - p)(b - a)}{D_c - \epsilon \mu_{\mathrm{ss}} / \beta d_c}$. (8)

Use of these parameters is based on the assumption of velocity weakening materials. Hence the approach has limited applicability for the majority of this data set, which is dominated by velocity strengthening characteristics. However, the velocity strengthening behaviour and lack of unstable slip may be, in part, an effect of the low temperature conditions of the tests. The aseismic creep observed for clay-bearing material in rock deformation experiments is at odds with the observations that most mature (and hence likely clay-bearing)

fault zones are also seismogenic (e.g. Chester et al., 1993; Jefferies et al., 2006; Logan and Chester, 1987; Toy et al., 2015; Wibberley and Shimamoto, 2003). A limited quantity of experimental data indicate that clay-bearing gouges become less stable with increasing temperature (Boulton et al., 2013; den Hartog et al., 2013;. Verbene et al., 2010).

The potential effect of compaction weakening is not considered in most stability analyses. Faulkner et al. (2018) showed that compaction of gouge in experiments can produce pore pressure transients that affect the gouge mechanical strength and also the determination of the rate and state parameters. In nature, if porosity is 'reset' due to fluidization in earthquakes, there is potential for compaction to occur with fault slip during earthquake nucleation . The dilatancy effects described in this work, produced by slip velocity changes, would be superimposed on these slip dependent porosity changes. Consequently, the interplay of compaction and dilatancy has the potential to produce quite complex pore pressure development during accelerating fault slip.

5 Conclusions

A series of velocity-step deformation experiments were conducted on synthetic quartz-kaolinite fault gouges to investigate the controls on pore volume changes in fault gouges. The kaolinite content in the gouges was controlled at 10 wt% increments to test the effect of composition on the frictional strength, stability and dilatancy of the gouges. The pressure conditions were set at 60 MPa, 25 MPa and 10 MPa $_{n}{}^{eff}$ to simulate a fault system at hydrostatic to overpressured conditions. The experimental results include that:

- All of the quartz-kaolinite gouges experienced dilation in response to an increase in slip velocity and compaction in response to a decrease in slip velocity.
- The scale of dilatancy in response to velocity-step changes was affected by the gouge kaolinite content but not by the effective stress conditions.
- Increasing kaolinite content in the synthetic gouges decreased the gouge frictional strength and increased (a-b) to promote stable sliding rather than unstable, earthquake slip.
- Increasing effective normal stress increased the likelihood of nucleation of unstable slip by decreasing the rate and state friction parameter (a-b).

Acknowledgments

We acknowledge financial support from a Natural Environment Research Council grant NE/V011804/1 to DRF and the NERC EAO DTP studentship to IRA at the University of Liverpool. Gary Coughlan and Michael Allen provided essential technical support in the maintenance and construction of the experimental apparatus. We gratefully acknowledge the Albert Crewe Centre for Electron Microscopy SEM SRF for their technical support, training & assistance in this research.

Open Research

The code and functions used for dilatancy volumometry analysis in the study are available on GitHub via https://github.com/izzyashman/rock-friction-dilatancy.git with a MIT License.

References

Audet, P., Bostock, M.G., Christensen, N.I., Peacock, S.M., 2009. Seismic evidence for overpressured subducted oceanic crust and megathrust fault sealing. Nature 457, 76–78.

Bedford, J.D., Faulkner, D.R., 2021. The Role of Grain Size and Effective Normal Stress on Localization and the Frictional Stability of Simulated Quartz Gouge. Geophys. Res. Lett. 48.

Bernabé, Y., Mok, U., Evans, B., 2006. A note on the oscillating flow method for measuring rock permeability. Int. J. Rock Mech. Min. Sci. 43, 311–316.

Boulton, C., Moore, D. E., Lockner, D. A., Toy, V. G., Townend, J., and Sutherland, R., 2014. Frictional properties of exhumed fault gouges in DFDP-1 cores, Alpine Fault, New Zealand. Geophys. Res. Lett., 41, 356– 362.

Brantut, N., 2020. Dilatancy-induced fluid pressure drop during dynamic rupture: Direct experimental evidence and consequences for earthquake dynamics. Earth Planet. Sci. Lett. 538, 116179.

Brown, K.M., Kopf, A., Underwood, M.B., Weinberger, J.L., 2003. Compositional and fluid pressure controls on the state of stress on the Nankai subduction thrust: A weak plate boundary. Earth Planet. Sci. Lett. 214, 589–603.

Byerlee, J.D., 1978. Friction of Rocks. Pageoph 116, 615–626.

Chester, F.M., Evans, J.P., Biegel, R.L., 1993. Internal structure and weakening mechanisms of the San Andreas Fault. J. Geophys. Res. 98, 771–786.

Crawford, B.R., Faulkner, D.R., Rutter, E.H., 2008. Strength, porosity, and permeability development during hydrostatic and shear loading of synthetic quartz-clay fault gouge. J. Geophys. Res. Solid Earth 113, 1–14.

Dal Zilio, L., Lapusta, N., Avouac, J.P., 2020. Unraveling Scaling Properties of Slow-Slip Events. Geophys. Res. Lett. 47.

S.A.M. den Hartog, A.R. Niemeijer, C.J. Spiers, 2013. Friction on subduction megathrust faults: Beyond the illite–muscovite transition. Earth Planet. Sci. Lett. Volume 373, 8-19.

Dieterich, J.H., 1979. Modeling of rock friction 1. Experimental results and constitutive equations. J. Geophys. Res. Solid Earth 84, 2161–2168.

Faulkner, D.R., Lewis, A.C., Rutter, E.H., 2003. On the internal structure and mechanics of large strike-slip fault zones: Field observations of the Carboneras fault in southeastern Spain. Tectonophysics 367, 235–251.

Faulkner, D.R., Rutter, E.H., 2000. Comparisons of water and argon permeability in natural clay-bearing fault gouge under high pressure at 20°C. J. Geophys. Res. Solid Earth 105, 16415–16426.

Faulkner, D.R., Sanchez-Roa, C., Boulton, C., den Hartog, S.A.M., 2018. Pore Fluid Pressure Development in Compacting Fault Gouge in Theory, Experiments, and Nature. J. Geophys. Res. Solid Earth 123, 226–241.

Ferdowsi, B., Rubin, A.M., 2020. A Granular Physics-Based View of Fault Friction Experiments. J. Geophys. Res. Solid Earth 125, 1–32.

Frank, W.B., Shapiro, N.M., Husker, A.L., Kostoglodov, V., Bhat, H.S., Campillo, M., 2015. Along-fault pore-pressure evolution during a slow-slip event in Guerrero, Mexico. Earth Planet. Sci. Lett. 413, 135–143.

French, M.E., Chester, J.S., 2018. Localized Slip and Associated Fluidized Structures Record Seismic Slip in Clay-Rich Fault Gouge. J. Geophys. Res. Solid Earth 123, 8568–8588.

Giorgetti, C., Carpenter, B.M., Collettini, C., 2015. Frictional behavior of talc-calcite mixtures. J. Geophys. Res. Solid Earth 120, 6614–6633.

Heimisson, E.R., Rudnicki, J., Lapusta, N., 2021. Dilatancy and Compaction of a Rate-and-State Fault in a Poroelastic Medium: Linearized Stability Analysis. J. Geophys. Res. Solid Earth 126, 1–28.

Ikari, M.J., Ito, Y., Ujiie, K., Kopf, A.J., 2015. Spectrum of slip behaviour in Tohoku fault zone samples at plate tectonic slip rates. Nat. Geosci. 8, 870–874.

Ikari, M.J., Saffer, D.M., Marone, C., 2007. Effect of hydration state on the frictional properties of montmorillonite-based fault gouge. J. Geophys. Res. Solid Earth 112, 1–12.

Ikari, M.J., Saffer, D.M., Marone, C., 2009. Frictional and hydrologic properties of clay-rich fault gouge. J. Geophys. Res. Solid Earth 114, 1–18.

Jefferies, S.P., Holdsworth, R.E., Wibberley, C.A.J., Shimamoto, T., Spiers, C.J., Niemeijer, A.R., Lloyd, G.E., 2006. The nature and importance of phyllonite development in crustal-scale fault cores: An example from the Median Tectonic Line, Japan. J. Struct. Geol. 28, 220–235.

Kodaira, S., Iidaka, T., Kato, A., Park, J.O., Iwasaki, T., Kaneda, Y., 2004. High pore fluid pressure may cause silent slip in the Nankai Trough. Science (80-.). 304, 1295–1298.

Kranz, R.L., Saltzman, J.S., Blacic, J.D., 1990. Hydraulic diffusivity measurements on laboratory rock samples using an oscillating pore pressure method. Int. J. Rock Mech. Min. Sci. 27, 345–352.

Li, Q., Tullis, T.E., Goldsby, D., Carpick, R.W., 2011. Frictional ageing from interfacial bonding and the origins of rate and state friction. Nature 480, 233–236.

Liu, Y., 2013. Numerical simulations on megathrust rupture stabilized under strong dilatancy strengthening in slow slip region. Geophys. Res. Lett. 40, 1311–1316.

Lockner, D.A., Byerlee, J.D., 1994. Dilatancy in hydraulically isolated faults and the suppression of instability. Geophys. Res. Lett. 21, 2353–2356.

Logan, J.M., Chester, F.M., 1987. Composite planar fabric of gouge from Punchbowl Fault, California.pdf. J. Struct. Geol. 9, 621–634.

Logan, J.M., Rauenzahn, K.A., 1987. Frictional dependence of gouge mixtures of quartz and montmorillonite on velocity, composition and fabric. Tectonophysics 144, 87–108.

Lupini, J.F., Skinner, A.E., Vaughan, P.R., 1981. The drained residual strength of cohesive soils. Geotechnique 31, 181–213.

Mair, K., Marone, C., 1999. Friction of simulated fault gouge for a wide range of velocities and normal stresses. J. Geophys. Res., 104(B12), 28899– 28914.

Marion, D., Nur, A., Yin, H., Han, D., 1992. Compressional velocity and porosity in sand-clay mixtures. Geophysics 57, 554–563.

Mead, W.J., 1925. The Geologic Role of Dilatancy. J. Geol. 33, 685–698.

Mitchell, T.M., Faulkner, D.R., 2008. Experimental measurements of permeability evolution during triaxial compression of initially intact crystalline rocks and implications for fluid flow in fault zones. J. Geophys. Res. Solid Earth 113, 1–16.

Moore, D.E., Lockner, D.A., 2011. Frictional strengths of talc-serpentine and talc-quartz mixtures. J. Geophys. Res. Solid Earth 116, 1–17.

Morrow, C.A., Byerlee, J.D., 1989. Experimental studies of compaction and dilatancy during frictional sliding on faults containing gouge. J. Struct. Geol. 11, 815–825.

Morrow, C.A., Moore, D.E., Lockner, D.A., 2017. Frictional strength of wet and dry montmorillonite. J. Geophys. Res. Solid Earth 122, 3392–3409.

Morrow, C.A., Shi, L.Q., Byerlee, J.D., 1984. Permeability of fault gouge under confining pressure and shear stress. J. Geophys. Res. 89, 3193–3200.

Noda, H., Shimamoto, T., 2009. Constitutive properties of clayey fault gouge from the Hanaore fault zone, southwest Japan. J. Geophys. Res. Solid Earth 114, 1–29.

Obara, K., Kato, A., 2016. Connecting slow earthquakes to huge earthquakes. Science 353, 253–257.

Ougier-Simonin, A., Zhu, W., 2013. Effects of pore fluid pressure on slip behaviors: An experimental study. Geophys. Res. Lett. 40, 2619–2624.

Peng, Z., Gomberg, J., 2010. An integrated perspective of the continuum between earthquakes and slow-slip phenomena. Nat. Geosci. 3, 599–607.

Proctor, B., Lockner, D.A., Kilgore, B.D., Mitchell, T.M., Beeler, N.M., 2020. Direct Evidence for Fluid Pressure, Dilatancy, and Compaction Affecting Slip in Isolated Faults. Geophys. Res. Lett. 47.

Pruett, R.J., Webb, H.L., 1993. Sampling and analysis of Kga-1B well-crystallized kaolin source clay. Clays Clay Miner. 41, 514–519.

Rathbun, A.P., Marone, C., 2010. Effect of strain localization on frictional behavior of sheared granular materials. J. Geophys. Res. 115, 1–16.

Rathbun, A.P., Marone, C., 2013. Symmetry and the critical slip distance in rate and state friction laws. J. Geophys. Res. Solid Earth 118, 3728–3741.

Reynolds, O., 1885. On the dilatancy of media composed of rigid particles in contact. With experimental illustrations. London, Edinburgh, Dublin Philos. Mag. J. Sci. 20, 469–481.

Rubin, A.M., 2008. Episodic slow slip events and rate-and-state friction. J. Geophys. Res. Solid Earth 113, 1–18.

Rudnicki, J.W., Chen, C.H., 1988. Stabilization of rapid frictional slip on a weakening fault by dilatant hardening. J. Geophys. Res. 93, 4745–4757.

Ruggieri, R., Scuderi, M.M., Trippetta, F., Tinti, E., Brignoli, M., Mantica, S., Petroselli, S., Osculati, L., Volontè, G., Collettini, C., 2021. The role of shale content and pore-water saturation on frictional properties of simulated carbonate faults. Tectonophysics 807, 1–12.

Ruina, A., 1983. Slip instability and state variable friction laws. J. Geophys. Res. 88, 10359–10370.

Rutter, E.H., Hackston, A.J., Yeatman, E., Brodie, K.H., Mecklenburgh, J., May, S.E., 2013. Reduction of friction on geological faults by weak-phase smearing. J. Struct. Geol. 51, 52–60.

Saffer, D.M., Marone, C., 2003. Comparison of smectite- and illite-rich gouge frictional properties: Application to the updip limit of the seismogenic zone along subduction megathrusts. Earth Planet. Sci. Lett. 215, 219–235.

Saffer, D.M., Wallace, L.M., 2015. The frictional, hydrologic, metamorphic and thermal habitat of shallow slow earthquakes. Nat. Geosci. 8, 594–600.

Samuelson, J., Elsworth, D., Marone, C., 2009. Shear-induced dilatancy of fluid-saturated faults: Experiment and theory. J. Geophys. Res. Solid Earth 114, 1–15.

Sánchez-Roa, C., Jiménez-Millán, J., Abad, I., Faulkner, D.R., Nieto, F., García-Tortosa, F.J., 2016. Fibrous clay mineral authigenesis induced by fluid-rock interaction in the Galera fault zone (Betic Cordillera, SE Spain) and its influence on fault gouge frictional properties. Appl. Clay Sci. 134, 275–288.

Segall, P., Rice, J.R., 1995. Dilatancy, compaction, and slip instability of a fluid-infiltrated fault. J. Geophys. Res. 100, 155–171.

Segall, P., Rubin, A.M., Bradley, A.M., Rice, J.R., 2010. Dilatant strengthening as a mechanism for slow slip events. J. Geophys. Res. Solid Earth 115, 1–37.

Skarbek, R.M., Savage, H.M., 2019. RSFit3000: A MATLAB GUI-based program for determining rate and state frictional parameters from experimental data. Geosphere 15, 1665–1676.

Takahashi, M., Mizoguchi, K., Kitamura, K., Masuda, K., 2007. Effects of clay content on the frictional strength and fluid transport property of faults. J. Geophys. Res. Solid Earth 112.

Tembe, S., Lockner, D.A., Wong, T.F., 2010. Effect of clay content and mineralogy on frictional sliding behavior of simulated gouges: Binary and ternary mixtures of quartz, illite, and montmorillonite. J. Geophys. Res. Solid Earth 115, 1–22.

Toy, V.G., Boulton, C.J., Sutherland, R., Townend, J., Norris, R.J., Little, T.A., Prior, D.J., Mariani, E., Faulkner, D., Menzies, C.D., Scott, H., Carpenter, B.M., 2015. Fault rock lithologies and architecture of the central Alpine fault, New Zealand, revealed by DFDP-1 drilling. Lithosphere 7, 155–173.

Verberne, B.A., He, C., Spiers, C.J., 2010. Frictional Properties of Sedimentary Rocks and Natural Fault Gouge from the Longmen Shan Fault Zone, Sichuan, China. Bulletin of the Seismological Society of America, 100 (5B), 2767–279.

Vogt, C., Lauterjung, J., Fischer, R.X., 2002. Investigation of the clay fraction (<2 m) of the clay minerals society reference clays. Clays Clay Miner. 50, 388–400.

von Terzhagi, K., 1936. The shearing resistance of saturated soils and the angle between the planes of shear. First Int. Conf. Soil Mech. 1, 54–56.

Wibberley, C.A.J., Shimamoto, T., 2003. Internal structure and permeability of major strike-slip fault zones. J. Struct. Geol. 25, 59–78.

Williams, J.C., 1968. The mixing of dry powders. Powder Technol. 2, 13–20.

Zhang, F., An, M., Zhang, L., Fang, Y., Elsworth, D., 2020. Effect of mineralogy on friction-dilation relationships for simulated faults: Implications for permeability evolution in caprock faults. Geosci. Front. 11, 439–450.